ResearchGate

See discussions, stats, and author profiles for this publication at: https://www.researchgate.net/publication/233328095

1 H -Pyrrolo[3,2- h]quinoline: A Benchmark Molecule for Reliable Calculations of Vibrational Frequencies, IR Intensities, and Raman Activities

ARTICLE *in* THE JOURNAL OF PHYSICAL CHEMISTRY A · NOVEMBER 2012

Impact Factor: 2.69 · DOI: 10.1021/jp309618b · Source: PubMed

CITATIONS
2

READS
20

7 AUTHORS, INCLUDING:

Alexandr Gorski
Instytut Chemii Fizycznej PAN
31 PUBLICATIONS **290** CITATIONS
SEE PROFILE

Sylwester Gawinkowski
ICFO Institute of Photonic Sciences
27 PUBLICATIONS **113** CITATIONS
SEE PROFILE

J. Waluk
Polish Academy of Sciences
258 PUBLICATIONS **3,724** CITATIONS
SEE PROFILE

Available from: Sylwester Gawinkowski
Retrieved on: 31 January 2016

THE JOURNAL OF PHYSICAL CHEMISTRY A

Article

pubs.acs.org/JPCA

1*H*-Pyrrolo[3,2-*h*]quinoline: A Benchmark Molecule for Reliable Calculations of Vibrational Frequencies, IR Intensities, and Raman Activities

Alexandr Gorski,[†] Sylwester Gawinkowski,[†] Jerzy Herbich,[†] Oliver Krauss,[‡] Bernhard Brutschy,[‡] Randolph P. Thummel,[§] and Jacek Waluk*[,†]

[†]Institute of Physical Chemistry, Polish Academy of Sciences, Kasprzaka 44/52, Warsaw 01-224, Poland

[‡]Institut für Physikalische und Theoretische Chemie, Goethe-Universität, Max-von-Laue-str. 7, 60438 Frankfurt am Main, Germany

[§]Department of Chemistry, University of Houston, Houston, Texas 77204-5003, United States

ABSTRACT: Reliable assignment of 55 out of 57 vibrational modes has been achieved for 1*H*-pyrrolo[3,2-*h*]quinoline using IR, Raman, and fluorescence spectroscopy combined with quantum chemical calculations. The experiments provided a data set for assessing the performance of different models/basis sets for predicting the vibrational frequencies, as well as IR and Raman intensities for a molecule with 13 heavy atoms. Among six different tested DFT functionals, the hybrid B3LYP used with Pople's split-valence basis sets is suggested as the best choice for accurate and cost-effective IR/Raman spectral simulations. Neither HF nor MP2 methods can satisfactorily describe the vibrational structure. Increasing the basis set size from double to triple-ζ and by adding polarization and diffuse functions does not necessarily improve the results, especially regarding the predictions of vibrational frequencies. With respect to the intensities, extending the basis set helps, with the accuracy increasing systematically for the Raman spectra, and in a less regular fashion for the IR. A large difference in accuracy is observed while comparing the spectral parameters predicted for in-plane and out-of-plane normal modes. The former are reliably computed with modest basis sets, whereas for the out-of-plane vibrations, larger basis sets are necessary, but even in this case, the out-of-plane vibrations are reproduced with much less accuracy than in-plane modes. This effect is general, as it has been observed using different functionals and basis sets.

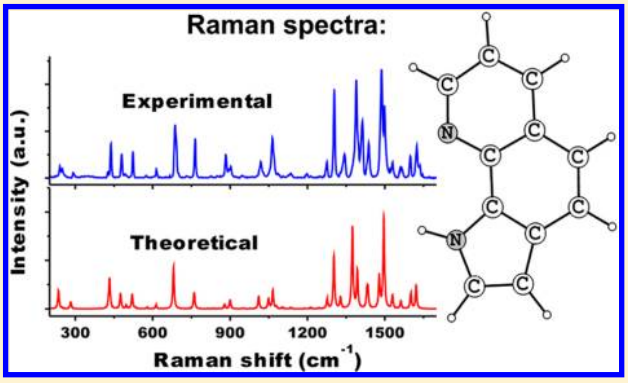

1. INTRODUCTION

Calculation of vibrational frequencies and intensities is one of the most useful and popular chemical tools offered to experimentalists by theory. Advances in theoretical models, especially those based on density functional theory (DFT), coupled with constantly increasing computer power make it now possible to obtain vibrational patterns and provide assignments for large organic molecules. In practice, such calculations always require a compromise between the desired accuracy and affordable costs. Therefore, of crucial importance is the proper choice of the computational method that would ensure reliable vibrational assignments. The usual approach is to compare the values obtained by different theoretical models with the available experimental data, possibly for a large set of molecules.[1−9] For instance, Schlegel and co-workers[4] have compared vibrational frequencies calculated at six different levels of theory with 900 experimental frequencies of 111 molecules, taken from the NIST Standard Reference Database. Comparing literature data obtained from different sources unavoidably introduces errors due to different experimental conditions of recording the spectra, calibrations of spectrometers, etc. These are, however, of the order of a few wavenumbers and become important only when extremely high accuracy of calculations is being tested.

Much more fundamental obstacles are encountered while trying to extend the reference database to larger molecules. First, higher CPU/memory requirements impose limitations on models/basis sets that can be used in practice. The second, most important issue concerns correct vibrational assignments. Reliable assignments are usually not a problem for small molecules, but become very difficult, or at least not unambiguous, when the number of heavy atoms exceeds a dozen or so. Therefore, the crucial factor for testing the performance of different theoretical models is finding a consistent set of accurately determined and properly assigned vibrational frequencies, along with the corresponding IR and Raman transition intensities, all of these measured under the same experimental conditions in a possibly inert environment.

Received: September 27, 2012
Revised: November 6, 2012
Published: November 7, 2012

ACS Publications © 2012 American Chemical Society

In this work, we propose such an approach. As a model object, we have selected 1*H*-pyrrolo[3,2-*h*]quinoline (PQ, Chart 1).

Chart 1. 1*H*-Pyrrolo[3,2-*h*]quinoline (PQ), Its 1:1 (a) and 1:2 (b) Complexes with Water/Alcohol, and Dimers (c)

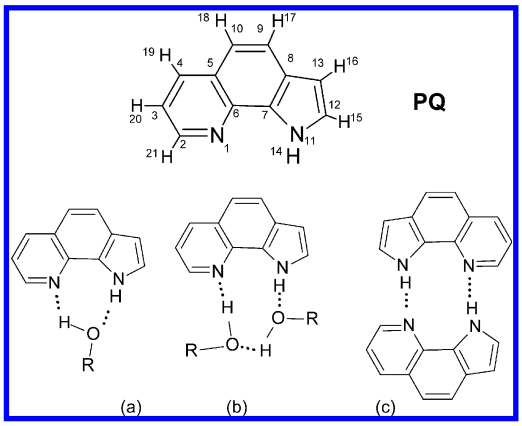

This molecule, possessing both hydrogen bond (HB) donor and acceptor groups, is becoming a role model in the studies of structure and reactivity in intermolecularly H-bonded complexes.[10−23] The proton donor, NH group, and the acceptor, pyridine nitrogen, are located three bonds apart, a distance that precludes formation of a strong intramolecular HB. The opposite situation is encountered in the intermolecularly H-bonded complexes with bifunctional HB donor/acceptor partners, such as water or alcohol (Chart 1a,b). Complexes of PQ with water and methanol have been found both for bulk solutions[11] and for molecules isolated in supersonic jets.[19−21] Cyclic structures seem to be preferred for both 1:1 and 1:2 complexes. Interestingly, photophysical properties are very different for the two stoichiometries. In 1:1 complexes, the excited singlet state is rapidly deactivated by excited state double proton transfer, occurring within single picoseconds.[14] The photoinduced reaction leads to a tautomeric form emitting strongly red-shifted fluorescence. In 1:2 species, another deactivation channel is the fastest: the S_1 state is depopulated by internal conversion to the ground state. The process occurs on the time scale of tens to hundreds of picoseconds and is strongly dependent on the viscosity of the environment, which suggests that a large amplitude motion is involved.[15]

Yet another pathway of excited state deactivation has been found for singly H-bonded complexes of PQ with heteroazaaromatic compounds, such as pyridine or quinoline.[16] Here, photoinduced electron transfer between the two moieties has been postulated.

PQ can also form HB-dimers. The literature X-ray data indicate a nonplanar structure, with the two moieties tilted with respect to each other.[24] Our crystallographic studies[25] show that the molecule can also crystallize in the form of planar, cyclic, doubly H-bonded dimers (Chart 1c). For such a structure, it is possible to envisage the possibility of excited state double proton transfer. Such a reaction has been thoroughly studied for 7-azaindole dimers, with controversies arising with respect to the mechanism of photoinduced tautomerization (synchronous vs stepwise transfer of protons).[26−32]

For a detailed description of tautomerization in intermolecularly H-bonded complexes or dimers, the knowledge of the vibrational structure is absolutely essential. The multidimensional character of proton/hydrogen transfer path seems to be a rule rather than an exception. We have recently demonstrated vibrational mode-selectivity for ground and excited state tautomerization in porphycene[33] and for 2-(2′-pyridyl)pyrrole.[34] In both cases, the reaction occurred along intramolecular HBs.

The present work is divided into two parts. In the first, a detailed characterization of the vibrational structure of PQ is obtained from the combination of quantum chemical calculations and IR, Raman, and fluorescence spectroscopies. Reliable assignments of 55 out of 57 vibrations of PQ are presented. In the second part, these data are used as a base for testing the accuracy of different theoretical methods in predicting vibrational frequencies, as well as IR and Raman intensities.

2. METHODOLOGY

2.1. Computations. The advantages of applying DFT methods for vibrational structure calculations have long been recognized. The best results are obtained using hybrid functionals. Becke three-parameter functional[35] with the Lee−Yang−Parr correlation functional[36] is the usual model of choice.[37] We therefore mainly used B3LYP, to assess its performance in combination with various basis sets. We also checked the accuracy of the "Coulomb-attenuating method" version of B3LYP, CAM-B3LYP.[38] This choice was dictated by our plans to analyze in the future the vibrational structure of PQ in the lowest excited singlet state, which is known to be of polar character. CAM-B3LYP is expected to perform well in such a case. In order to check the general character of the conclusions of this work, we also performed calculations using other functionals, including those using local spin density approximation (LSDA), generalized gradient approximation (GGA), hybrid, and global-hybrid meta-GGA ones: SVWN,[39−42] PBE,[43] PBE0,[43,44] and M06.[45]

In addition to DFT models, HF and MP2[46] calculations have also been performed. The following basis sets have been used: 6-31G,[47] 6-31G(d),[48,49] 6-31+G(d),[50] 6-31G(d,p),[49] 6-31+G(d,p),[47,51] 6-31++G(d,p),[47,51] 6-311G(d),[52] 6-311+G(d),[51,52] 6-311G(d,p),[52] 6-311+G(d,p),[50] and 6-311G++(d,p).[51,52] Both double-ζ (DZ) and triple-ζ (TZ) basis functions were also augmented with additional d- and f-type functions on heavy atoms and p and d functions on hydrogens. The following combinations were tested: 6-31+G(2d,p), 6-31+G(2d,2p), 6-31+G(3d,3p), 6-31+G(3df,3pd), 6-31++G(3df,3pd), 6-311+G(2d,p), 6-311+G(2d,2p), 6-311+G(3d,3p), 6-311+G(3df,3pd), and 6-311++G(3df,3pd).[50−52] Calculations were also performed using Dunning's "correlation consistent" basis sets:[53] cc-pVDZ, aug-cc-pVDZ, cc-pVTZ, aug-cc-pVTZ, and cc-pVQZ. Finally, we also tested Sadlej's pVTZ[54] and Z3PolX,[55] recommended for calculations of molecular electric properties.

All the calculations were performed using Gaussian 09.[56] In order to ensure adequate convergence and reliability of the computed frequencies, Opt = Tight option was used, together with Int = UltraFine in the case of DFT calculations. Two sets of calculations were performed for each model/basis set combination, one without imposing the symmetry, and the other enforcing the planarity. In order to convert the calculated Raman activities into quantities comparable with the experimental results, they were multiplied by a factor of $((12738.9 - \nu)^4/\nu)/10^{12}$.[1] In this equation, 12738.9 is the wavenumber corresponding to the laser wavelength used to record the spectra (785 nm), and ν (in cm^{-1}) is the calculated transition frequency (after applying the scaling factor). As the spectra were measured at 10 K, no temperature correction was necessary.

dx.doi.org/10.1021/jp309618b | J. Phys. Chem. A 2012, 116, 11973−11986

The vibrational transitions were computed within the harmonic approximation. In one case, the results were compared with those obtained using anharmonic calculations[57] (Gaussian option freq = anharmonic).

Simulations of rare gas matrix-induced shifts of vibrational peaks were carried out using the polarized continuum model (PCM).[58] (Gaussian option SCRF(PCM, Solvent = Argon)).

2.2. Experimental Section. Synthesis and purification of PQ was carried out according to procedures described earlier.[59]

Crucial for the purpose of this work are IR and Raman spectra obtained for low-temperature inert matrix. Samples of PQ isolated in argon matrices were obtained using a closed-cycle helium cryostat (CSW-202N, Advanced Research Systems). The compound was heated in a glass tube and codeposited with argon at a ratio of about 1:1000 onto a cold (20 K) KBr window mounted in a cryostat with 10^{-6} Torr background pressure. During measurements of both IR and Raman spectra, the matrix temperature was kept at 10 K.

The IR spectra were recorded with 1 cm^{-1} resolution on a Nicolet Magna 560 FTIR spectrometer, equipped with an MCT/B liquid-nitrogen-cooled detector. In addition to the measurements in Ar matrix, the IR spectra were also recorded for room temperature dichloromethane (DCM) solutions and for the gas phase. The gas-phase experiments were carried out in a homemade high-temperature chamber. PQ powder, contained in a 10 cm long IR cuvette, was heated to 400 K, which allowed to reach the pressure of PQ vapor sufficient for IR measurements. Comparison of IR spectra obtained at different temperatures in various environments served several purposes: (i) it allowed a double check of the vibrational frequencies, which was particularly important for weak transitions; it demonstrated (ii) negligible frequency shifts and (iii) minor intensity variations for PQ in different environments. Most important, it also allowed one to distinguish between peaks due to different vibrational transitions from those caused by site-splittings observed for some transitions in an argon matrix.

For the measurements of Raman spectra, a Renishaw InVia microscopic system was used. In order to account for the dependence of the spectrometer sensitivity on wavelength, the Raman instrument was calibrated with a Bentham CL2 spectral irradiance standard lamp. Three excitation sources were used: (i) an HPNIR785 diode laser emitting at 785 nm; (ii) Stellar Pro Modu-Laser (LLC) emitting the Ar^+ 514.5 nm line, and (iii) a 632.8 nm He−Ne laser (Renishaw RL633). The laser light was focused on a sample with a 60 mm focusing distance objective. The laser power at the sample was 5 mW or less. The Raman-scattered light was collected by the same objective through a cutoff filter to eliminate Rayleigh scattering. Gratings of 1800 and 1200 grooves/mm were used for 514.5 and 785 nm laser lines, respectively. The resolution was 5 cm^{-1} and the wavenumber accuracy 2 cm^{-1}, both calibrated with the Rayleigh line and the 520.6 cm^{-1} line of silicon. The Raman spectra were recorded by a 1024 × 256 pixel Peltier-cooled RenCam CCD detector.

Supersonic jet investigations were performed with an experimental setup described in more detail elsewhere.[60,61] Briefly, PQ was seeded into a helium expansion through a pulsed nozzle (General Valve Series 9) with either a 200 μm or a 500 μm orifice. The samples were typically heated to 400 K, and the stagnation pressure was between 2 and 3 bar. The jet-cooled molecules were probed by fluorescence excitation (FE) and dispersed fluorescence (DF) spectroscopy. The UV excitation was provided by the pulsed, frequency-doubled output of a Nd:YAG (Continuum Powerlite 8000) pumped optical parametric oscillator OPO (Continuum Sunlite) running at a repetition rate of 10 Hz. Fluorescence was collected with two lenses at right angles to both the jet and the laser beam. Before detection, the emission was dispersed by a spectrograph of 250 mm focal length (Chromex 250 IS). Two different detectors were used to analyze the dispersed light. A cooled CCD-camera coupled to an image intensifier (LaVision FI-III) served to obtain DF spectra with a resolution and spectral range (of about 250 nm) depending on the selected grating in the spectrograph. Alternatively, a side-on type photomultiplier tube (Hamamatsu R4220) behind an exit slit (with variable width) could be used to detect a selectable section of the emission spectrum of up to 30 nm bandwidth. This mode was used for recording FE spectra with a resolution of about 0.1 cm^{-1}, given by the bandwidth of the excitation laser. DF spectra were typically accumulated over 1000 laser shots, while FE were averaged over 100 shots.

3. VIBRATIONAL ASSIGNMENTS FROM IR, RAMAN, AND DISPERSED FLUORESCENCE SPECTRA

Figure 1 shows the IR and Raman spectra measured for PQ isolated in low-temperature argon matrix. This figure also

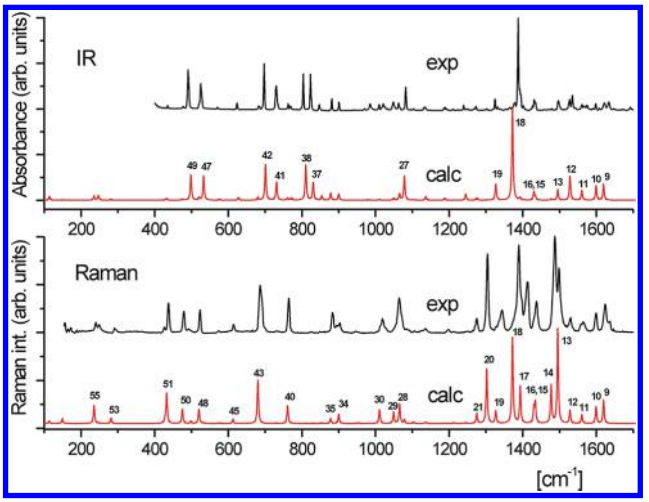

Figure 1. Top, IR, and bottom, Raman spectra measured for PQ isolated in Ar at 10 K. In red, theoretically predicted spectra, obtained by B3LYP/cc-PVQZ calculations, using a scaling factor of 0.9805. The numbering of vibrational modes corresponds to that of Table 1.

presents theoretically simulated spectra, obtained using B3LYP and a large basis set, cc-PVQZ. An excellent agreement is observed regarding both positions and intensities of most IR and Raman bands. We will show below that the spectra can be satisfactorily predicted using smaller basis sets, albeit with somewhat larger errors. The values of observed vibrational frequencies and relative IR and Raman intensities are given in Table 1. Inspection of Figure 1 reveals very different IR and Raman intensity patterns. Some strong bands are observed at very similar frequencies, but they correspond to different modes (e.g., the band located at 523 cm^{-1} in the Raman spectrum, corresponding to ν_{48} and the 526 cm^{-1} transition in the IR spectrum, corresponding to ν_{47}). Such situation is fortunate both for reliable assignments and for assessing the performance of theoretical models in predicting IR and Raman intensities.

The assignments presented in Table 1 are based on fulfilling several independent criteria. First, the experimentally observed and calculated vibrational patterns were compared with regard to band locations and intensities. Then, cross-correlations between

dx.doi.org/10.1021/jp309618b | J. Phys. Chem. A 2012, 116, 11973−11986

Table 1. Experimental IR and Raman Spectra vs Calculated Vibrational Frequencies, IR Intensities, and Raman Activities

	calculated[a]			observed							
				IR			Raman				
				Ar[b]		DCM[c]	Ar[b,d]		DCM[c]	Flu[e]	
	$\tilde{\nu}$	IR int	Raman act	$\tilde{\nu}$	int	$\tilde{\nu}$	$\tilde{\nu}$	int	$\tilde{\nu}$	$\tilde{\nu}$	assignment[f]
ν_1 (a′)	3588	82.62	75.59	3507	0.31				3456		NH str
				3501	0.58						
				3496	0.46						
ν_2 (a′)	3193	2.08	215.32	3131	0.07		3131		3132		s CH str
ν_3 (a′)	3174	2.69	100.71	3112	0.08		3114		3112		as CH str
ν_4 (a′)	3127	18.25	283.65	3076	0.14		3077				s CH str
ν_5 (a′)	3117	21.94	193.43				3069				s CH str
ν_6 (a′)	3100	10.86	145.84	3051	0.32		3052				as CH str
ν_7 (a′)	3098	0.90	1.25								as CH str
ν_8 (a′)	3077	23.97	156.33	3038	0.06		3041				as CH str
				3027	0.12						$\nu_{10} + \nu_{16}$, $\nu_{12} + \nu_{13}$
				2983	0.043						$\nu_{10} + \nu_{18}$, $2\nu_{13}$
				1938	0.031						$\nu_{22} + \nu_{42}$, $\nu_{25} + \nu_{38}$
				1915	0.024						$\nu_{18} + \nu_{47}$, $\nu_9 + \nu_{53}$
				1909							
				1884	0.031						$\nu_{18} + \nu_{49}$
				1764	0.013					1764	$\nu_{12} + \nu_{55}$
				1736	0.011					1728	$\nu_{13} + \nu_{55}$
				1692	0.036						$2\nu_{36}$
				1670	0.0094					1665	$\nu_{16} + \nu_{55}$
				1632	0.1	1627	1635		1628	1628	$\nu_{37} + \nu_{38}$, $2\nu_{37}$
ν_9 (a′)	1621	18.92	50.77	1621	0.18	1616	1624	0.41	1619		NH b, CC str cr
ν_{10} (a′)	1601	17.49	34.97	1598	0.093	1595	1599	0.20	1596		(CC, CN) str pyridine
ν_{11} (a′)	1562	12.11	17.30	1574		1564	1565	0.17	1560	1564	NH, CH b pyridine
				1567	0.12						
				1561							
						1558					$\nu_{37} + \nu_{41}$
ν_{12} (a′)	1529	29.98	24.76	1527	0.23	1534	1530	0.18	1525	1527	NH, CH18,20 b
				1534							
ν_{13} (a′)	1496	13.05	179.58	1496	0.21	1494	1498	0.73	1496	1495	NH b, CC str pyr
ν_{14} (a′)	1478	1.54	69.61	1489	<0.01	1487	1486	1.4	1484		CH20 s b, skel def CC
				1480	<0.01						$\nu_{29} + \nu_{51}$, $\nu_{31} + \nu_{49}$
ν_{15} (a′)	1435	3.77	32.79	1435	0.070		1437	0.45[x]		1436	NH, CH20,21 b, skel def pyr
ν_{16} (a′)	1431	10.48	27.21	1431	0.11	1429	1429	0.45[x]			CH17,18,19,20 b, CC str cr
							1413	0.80	1411		$\nu_{20} + \nu_{57}$
ν_{17} (a′)	1394	3.17	63.70	1396	0.096	1393	1398sh		1395		NH, CH21 b, skel def pyr
ν_{18} (a′)	1373	112.65	143.03	1388	1.0	1384	1389	1.46	1387	1382	CH17,18,19,20 b, CC str cr
							1344	0.21	1339		$\nu_{34} + \nu_{51}$
ν_{19} (a′)	1328	20.25	19.62	1325	0.12	1325	1328		1327		skel def, CH b
ν_{20} (a′)	1303	0.43	85.13	1302	0.027	1300	1304	0.81	1302	1295	skel def, CH as b
ν_{21} (a′)	1276	2.81	14.64	1273	0.041		1275	0.16			CH b, C7N11, C8C9 str
ν_{22} (a′)	1246	7.43	1.08	1239	0.053	1240	1241	<0.01	1243	1235	NH and CH b
ν_{23} (a′)	1212	0.16	1.36	1211	0.018	1209	1213	0.012			CH b, CC str cr
				1195	0.010		1198	0.055	1197	1192	$\nu_1 + \nu_{27}$
ν_{24} (a′)	1189	2.44	0.34	1186	0.052	1187					CH b, CC str
				1190							
ν_{25} (a′)	1138	4.35	1.84	1134	0.075	1135	1135	0.095		1135	CH17,18,19,20 b
ν_{26} (a′)	1104	0.58	1.90	1103	0.027	1104	1104	0.005	1105	1104	CH15,17,18,20 and NH b
ν_{27} (a′)	1080	29.54	3.80	1082	0.25	1080	1084	0.025	1080	1075	skel def, CH b
ν_{28} (a′)	1066	7.56	22.13	1063	0.11	1064	1064	0.75	1065		CH15,16 b
ν_{29} (a′)	1050	2.54	11.72	1048	0.16	1052			1053		skel def, CH b
				1021	0.096						$\nu_{47} + \nu_{49}$, $\nu_{41} + \nu_{53}$
ν_{30} (a′)	1012	0.85	14.56	1010	0.041	1012	1019	0.29	1014	1004	skel def
ν_{31} (a″)	976	0.70	0.25	985	0.12						CH19−21 s oop twisting
				970	0.010	976	964				$\nu_{41} + \nu_{55}$, $\nu_{49} + \nu_{50}$
ν_{32} (a″)	950	0.00	0.16	949	<0.01	948	953		950		CH17,18,21 oop twisting

dx.doi.org/10.1021/jp309618b | J. Phys. Chem. A 2012, 116, 11973−11986

Table 1. continued

	calculated[a]			observed							
				IR			Raman				
				Ar[b]		DCM[c]	Ar[b,d]		DCM[c]	Flu[e]	
	$\tilde{\nu}$	IR int	Raman act	$\tilde{\nu}$	int	$\tilde{\nu}$	$\tilde{\nu}$	int	$\tilde{\nu}$	$\tilde{\nu}$	assignment[f]
ν_{33} (a″)	945	0.19	0.82	942	0.013		946	0.036			CH17−19,21 oop twisting
ν_{34} (a′)	901	7.91	8.44	901	0.07		903	0.13		904	skel def pyr (N11−C12−C13)
ν_{35} (a′)	879	8.56	4.12	881	0.11	880	883	0.27	882		skel def
ν_{36} (a″)	849	6.57	0.27	847	0.064	858	849	0.013		843	CH15,16 and oop twisting
ν_{37} (a″)	829	19.30	0.34	824	0.38	827	826	0.020	828		skel oop def, CH wag
ν_{38} (a″)	809	42.82	0.05	804	0.31	803					cr oop def, CH as wag
ν_{39} (a″)	770	2.81	0.07	769	0.035						CH17−21 oop wag
ν_{40} (a′)	761	2.69	12.91	763	0.053		764	0.33		758	ip skel def
ν_{41} (a″)	729	21.13	0.11	730	0.38		731	0.016			CH15−18 oop s wag
ν_{42} (a″)	701	45.05	0.02	697	0.46		697	<0.01			oop skel def, CH wag
ν_{43} (a′)	681	3.03	26.85	683	0.048		687	0.70		679	cr and pyridine ring b (sym along N1−C4, C7−C10 axis)
ν_{44} (a″)	626	3.06	0.06	624	0.057	627					as NH, CH oop
ν_{45} (a′)	613	0.14	2.26	613	<0.01		614	0.076	614	611	cr and pyridine ring b (asym along N1−C4, C7−C10 axis)
ν_{46} (a″)	575	0.94	0.51	571	0.02	571	574	0.020			oop skel def pyridine and cr
ν_{47} (a″)	532	28.76	0.44	526	0.41	521					NH and skel def oop
ν_{48} (a′)	521	3.24	6.32	523	0.035	520	523	0.18	522	519	ip skel def pyridine and cr
ν_{49} (a″)	497	31.42	1.14	491	0.51		493	0.058			s NH, CH oop
ν_{50} (a′)	475	1.38	5.74	477	0.017		479	0.19	478	474	ip skel def cr
ν_{51} (a′)	433	2.01	10.17	436	0.028		438	0.27	437	432	ip skel def cr
ν_{52} (a″)	428	0.53	1.19	425	0.01		427	0.04			oop skel def cr, CH17,19 oop
ν_{53} (a″)	282	1.15	1.11				291	0.041			oop pyridine and cr rock
ν_{54} (a″)	247	5.84	0.09				249	0.12	249		oop pyr and cr rock
ν_{55} (a′)	235	5.10	2.43				240	0.10	240	236	pyr and pyridine rings ip bend
ν_{56} (a″)	150	0.64	0.31				156				pyr and pyridine tor
ν_{57} (a″)	114	4.65	0.09								oop pyridine and pyr rock

[a]B3LYP/cc-pVQZ, C_s symmetry group, scaling factor = 0.9805; frequencies in cm^{-1}, IR intensities in km/mol, Raman scattering activities in $Å^4$/amu. [b]At 10 K. [c]At 293 K. [d]With 785 nm laser (633 nm laser was used in the NH stretching region). [e]Supersonic jet. [f]Abbreviations: s, symmetric; as, antisymmetric; str, stretch; b, bend; ip, in-plane; oop, out-of-plane; skel def, skeletal deformation; tor, torsion; pyrid, pyridine; pyr, pyrrole; cr, central ring.

IR and Raman intensities were analyzed. Such a procedure enables, in particular, reliable assignments of close-lying vibrational transitions since the observed and predicted intensity patterns are very different for IR and Raman spectra. Additional help in the assignments was provided by comparing the IR spectra of PQ and its isotopologue for which the NH proton was replaced with a deuteron. The shifts of vibrational transitions upon deuteration are usually predicted with higher accuracy than the absolute positions; we checked, and this was indeed the case for PQ.

The results obtained for matrix-isolated PQ were also compared with the data provided by measurements in the gas phase, room temperature solutions of PQ in dichloromethane, and solid PQ, both crystalline and embedded in KBr pellets. Such analysis was useful to separate transitions due to different modes from those caused by site-splitting in an Ar matrix. Moreover, we took advantage of the fact that crystalline PQ consists not of monomeric units, but of H-bonded dimers. Vibrational patterns simulated for dimers were compared with those measured for solid PQ. Different modes in the monomer respond differently to dimerization: usually, frequency shifts are small, but intensity patterns may differ significantly, which helps in the assignments. A detailed analysis of vibrational structure of PQ dimers has been presented in a separate work.[25] Finally, the assignments were strengthened by measuring fluorescence of PQ isolated in a supersonic jet. Figure 2 presents the excitation spectrum, whereas Figure 3 shows examples of single vibronic level fluorescence (SVLF) spectra, obtained after exciting a particular

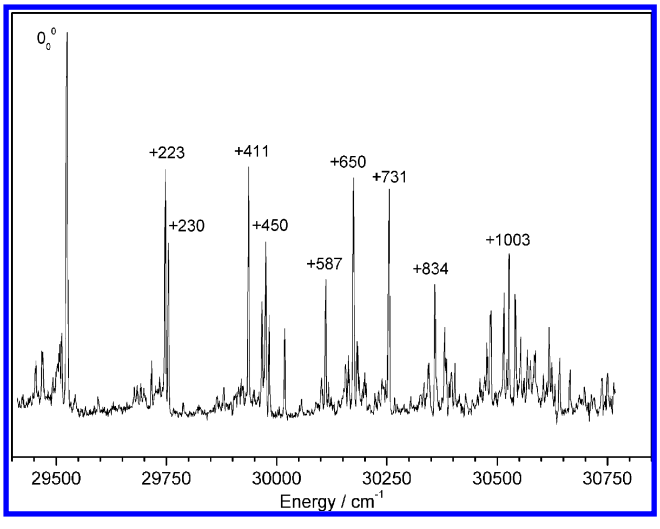

Figure 2. Excitation spectrum of fluorescence of PQ measured in a supersonic jet.

dx.doi.org/10.1021/jp309618b | J. Phys. Chem. A 2012, 116, 11973−11986

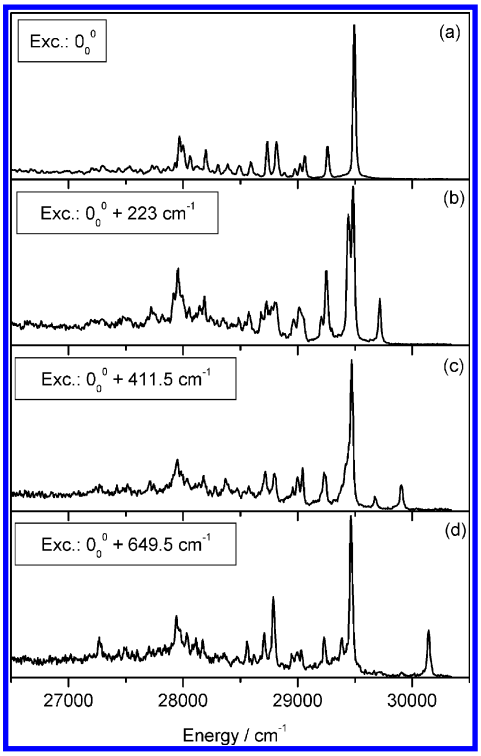

Figure 3. Single vibronic level fluorescence of PQ in a supersonic jet. The spectra correspond to the excitation into the 0−0 band (a) and into three vibronic transitions, corresponding to S_1 counterparts of ν_{55} (b), ν_{51} (c), and ν_{43} (d) (see Table 1).

mode in the S_1 electronic state. The analysis of excitation−emission patterns allows mapping of correlations between vibrational modes in the ground and excited electronic states. Such correlations will be discussed elsewhere. For the purpose of this work, we use the values of ground state frequencies observed in SVLF. They are included in Table 1.

On the basis of comparison of IR, Raman, and fluorescence spectra, combined with the results of calculations, we were able to reliably assign 55 of 57 PQ vibrations (Table 1). The only two missing ones are (i) one of the CH stretching modes, ν_7, for which the calculations predict low intensity in both IR and Raman spectra, and (ii) the lowest frequency mode, ν_{57}. Actually, for a crystalline PQ sample, we observed a Raman transition at 113 cm^{-1}, in very good agreement with calculations. However, solid PQ consists of doubly hydrogen-bonded dimers, and therefore, we refrained from assigning the value of 113 cm^{-1} to the monomer, even though the calculations performed for the dimer predict a very similar frequency, differing by only 2 cm^{-1}.

4. ASSESSING THE PERFORMANCE OF THEORETICAL MODELS

4.1. Calculations of Vibrational Frequencies. As the experimental data set to be used as a benchmark for testing various theoretical models, we selected all the fundamental frequencies except the high energy ones, i.e., those corresponding to CH and NH stretches. It is well-known that different scaling factors are usually applied for wavenumbers below and above 1800 cm^{-1}.[4] Moreover, the assignments of CH stretches are not complete and also less certain than those of the other modes. Thus, our data set consists of 48 frequency values, spanning the range of 150−1630 cm^{-1}: 31 of those are due to in-plane polarized (a′) transitions, whereas 17 correspond to out-of-plane (a″) vibrations (cf. Table 1).

Table 2 presents the statistics of calculations of vibrational frequencies performed for PQ using different models and various basis sets. The average mean differences (AMDs), absolute average mean differences (AAMDs), standard deviations (SDs), correlation coefficients (*R*s), and uniform scaling factors (λ) were obtained from a linear fit of the experimental data to the computed values: $\nu_{exptl} = \lambda\nu_{calcd}$. Figure 4 shows selected examples of this procedure.

The main sources of differences between experimental and predicted values are (i) the use of harmonic approximation; (ii) incomplete treatment of electron correlation, and (iii) a limited basis set. We checked that the effects of anharmonicity are not crucial for PQ by comparing the results of standard harmonic B3LYP/6-31G+(d) calculations with those of anharmonic calculations obtained using the same model and basis set. A perfect correlation between the two sets was observed: $\nu_{anh} = (1.00064 \pm 0.00027)\nu_{harm}$ ($r^2 = 0.99999$). The differences between computed anharmonic and harmonic frequencies did not exceed 5 cm^{-1}. The only exception was the NH stretching mode, for which the anharmonic frequency was lower by 16 cm^{-1}. This could be expected, since there is a possibility of a weak intramolecular hydrogen bonding between the NH group and the pyridine nitrogen atom.

Inspection of Table 2 shows that the DFT models with B3LYP functional yield extremely good predictions of the transition frequencies, especially when used with Pople's split-valence basis sets. Regarding the size of the basis set, already the modest 6-31+G(d) fares well, giving the standard deviation and the absolute average mean distance of less than 6 and 5 cm^{-1}, respectively. Passing from double to triple-ζ basis sets results in the SD and AAMD values smaller by about 1−2 cm^{-1} and thus comparable to the experimental uncertainty caused, on one hand, by the accuracy of the instrument and, on the other hand, by the fact that the spectra have not been measured in the vacuum. In this context, we note that the largest absolute difference between the predicted and measured values is observed for the most intense IR transition, ν_{18}. The calculations underestimate the frequency by more than 10 cm^{-1}. In the gas phase spectra, a red shift of 5 cm^{-1} is observed, making this difference half smaller. Other frequencies are shifted significantly less, indicating that the matrix effect is proportional to the oscillator strength of the transition. We tried to simulate the matrix shifts using the polarizable continuum model (PCM). The calculations, carried out at the 6-31G+(d) level predicted blue and red shifts not exceeding 2 cm^{-1}, the only exception being the NH stretching vibration (red shift of 46 cm^{-1}). Given that the calculations (i) did not reproduce the effect for the strongest IR transition and that (ii) they predicted very small absolute shifts, we did not try to refine our correlations by trying to apply the corrections due to matrix effects. Neither did we try to correct for possible intensity changes; comparison of the IR spectra recorded in the gas phase, solution, and Ar matrix suggests that these effects are not substantial.

Interestingly, increasing the size of the basis set does not necessarily improve the agreement between theory and experiment and can, in the case of double-ζ basis sets, lead to larger SD/AAMD values. This result indicates the importance of choosing a well-balanced basis set.

For the double-ζ basis sets, Pople's bases yield somewhat more accurate frequencies that Dunning's. For the triple-ζ case, both basis sets yield comparable results.

Table 2. Statistics for Vibrational Frequencies Calculated Using Different Models/Basis Sets

model	basis set	scale factor	corr coeff	stand dev[a]	av mean diff[a]	abs aver mean diff[a]	rel CPU time
HF	6-31G(d,p)	0.9020	0.99920	16.64	1.31	12.75	1.1
	6-311G(d,p)	0.9079	0.99909	17.45	0.79	13.56	4.3
MP2	cc-pVDZ	0.9824	0.99860	29.79	8.37	22.98	549.6
B3LYP	6-31G	0.9639	0.99956	13.06	−1.95	8.67	1.0
	6-31G(d)	0.9747	0.99989	7.64	1.79	6.13	2.6
	6-31+G(d)	0.9771	0.99992	5.80	1.11	4.77	3.0
	6-31+G(d)[b]	0.9774	0.99993	5.79	1.28	4.70	496.6
	6-31G(d,p)	0.9761	0.99992	6.31	1.42	4.85	4.4
	a′ only	0.9748	0.99995	5.43	1.30	4.34	
	a″ only	0.9841	0.99981	5.22	−0.36	4.05	
	6-31+G(d,p)	0.9791	0.99994	5.06	0.87	3.94	10.1
	6-31++G(d,p)	0.9790	0.99995	4.73	0.86	3.65	11.2
	6-31+G(2d,p)	0.9806	0.99993	5.18	0.56	4.09	18.0
	6-31+G(2d,2p)	0.9809	0.99993	4.74	0.34	3.73	20.7
	6-31+G(3d,3p)	0.9805	0.99993	4.75	0.24	4.02	40.5
	6-31+G(3df,3pd)	0.9819	0.99985	7.11	−0.54	5.61	77.7
	6-31++G(3df,3pd)	0.9818	0.99984	7.31	−0.58	5.81	82.4
	cc-pVDZ	0.9798	0.99987	6.65	0.48	5.66	3.8
	aug-cc-pVDZ	0.9816	0.99982	7.85	−0.45	6.28	36.2
	Z3PolX	0.9743	0.99881	21.73	−3.34	16.54	15.0
	Sadlej pVTZ	0.9743	0.99931	15.35	−1.09	11.46	31.8
	6-311G	0.9726	0.99950	14.80	−2.76	9.65	2.0
	6-311G(d)	0.9807	0.99987	7.24	1.23	4.88	4.5
	6-311+G(d)	0.9816	0.99992	6.02	1.18	4.50	10.7
	6-311G(d,p)	0.9817	0.99996	3.95	0.45	2.86	8.2
	a′ only	0.9817	0.99997	3.36	0.47	2.43	
	a″ only	0.9848	0.99983	4.80	0.23	3.75	
	6-311+G(d,p)	0.9827	0.99995	4.21	0.43	3.18	10.1
	6-311++G(d,p)	0.9831	0.99995	4.29	0.58	3.02	12.7
	6-311+G(2d,p)	0.9842	0.99993	5.78	1.24	4.44	28.2
	6-311+G(2d,2p)	0.9827	0.99994	4.88	0.68	3.52	33.2
	6-311+G(3d,3p)	0.9840	0.99995	4.67	0.75	3.43	39.2
	6-311+G(3df,3pd)	0.9815	0.99992	5.15	0.34	3.69	106.3
	6-311++G(3df,3pd)	0.9815	0.99992	5.08	0.34	3.68	111.5
	cc-pVTZ	0.9798	0.99995	4.16	0.09	3.15	39.5
	cc-pVTZ d_1[c]	0.9803	0.99992	4.26	−0.37	3.37	0.0
	aug-cc-pVTZ	0.9798	0.99988	6.34	−0.55	4.71	788.4
	cc-pVQZ	0.9805	0.99995	4.27	0.06	3.15	1110
	a′ only	0.9808	0.99995	3.89	0.21	2.70	
	a″ only	0.9786	0.99983	4.82	0.33	3.61	
CAM-B3LYP	6-31G(d,p)	0.9587	0.99982	8.64	1.59	6.69	3.5
CAM-B3LYP	Z3PolX	0.9570	0.99861	22.74	−2.89	17.94	23.1
CAM-B3LYP	cc-pVTZ	0.9628	0.99982	7.72	0.30	6.52	50.2
SVWN	6-311++G(d,p)	0.9550	0.99973	16.51	2.66	12.74	5.4
	cc-pVTZ	0.9929	0.99977	15.52	2.41	12.25	20.8
PBE	6-311++G(d,p)	1.0107	0.99991	9.73	1.82	6.81	10.0
	cc-pVTZ	1.0092	0.99994	8.12	1.44	5.75	28.4
PBE0	6-311++G(d,p)	0.9711	0.99994	7.75	1.91	6.45	13.0
	cc-pVTZ	0.9689	0.99996	6.51	1.41	5.36	52.0
M06	6-311++G(d,p)	0.9823	0.99992	8.87	2.10	7.01	19.5
	cc-pVTZ	0.9783	0.99996	7.35	1.20	5.79	60.6

[a]In cm^{-1}. [b]Anharmonic calculations. [c]Calculations for *N*-deuterated PQ.

The performance of Sadlej's pVTZ and Z3PolX basis sets is definitely worse. The values of SD and AMD, about 10−20 cm^{-1}, are practically the same as those reported earlier when testing these sets for a series of small molecules.[4,5,62] While such differences are acceptable for the assignment of vibrations in small molecules, they are too large for medium and large chromophores, where the spacing between various vibrational transitions often falls below 10 cm^{-1}.

Similar errors, exceeding 10 cm^{-1} but lower than 20 cm^{-1}, were obtained in the case of Hartree−Fock (HF) calculations, the agreement not improving upon passing from a double- to a triple-ζ basis set. As expected, the HF scaling factors are quite

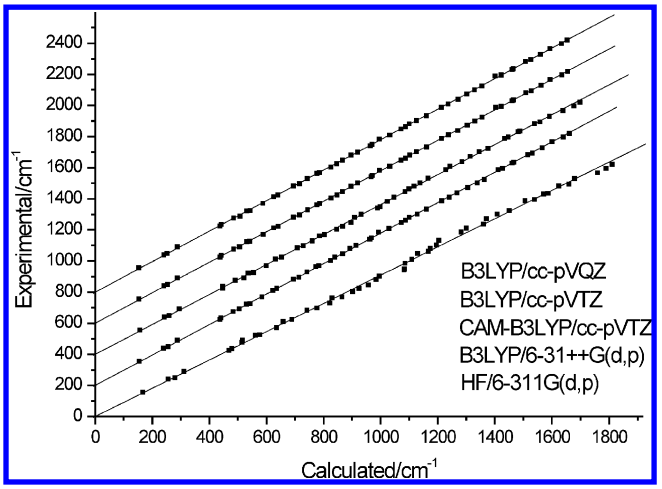

Figure 4. Selected examples of correlation between experimentally observed and calculated vibrational frequencies. For reasons of visibility, the curves have been shifted vertically by 200 cm^{-1} with respect to each other.

different from one. For DFT calculations, their values increase from about 0.96 to above 0.98 upon extending the basis set.

Comparison of B3LYP and CAM-B3LYP functionals shows a definitely better performance of the former, but the results obtained for the latter are also acceptable. This is reassuring in view of possible applications of CAM-B3LYP for predicting vibrational structure in the electronically excited states.

A remarkably poor performance was obtained in the case of MP2 calculations, regarding not only the errors in frequencies but also in predicted intensities. Such behavior, however, was not unexpected.[8] The inability of MP2 to properly reproduce the form of certain vibrational modes has been discussed before for such aromatic molecules as benzene[63−66] or phenol.[67] These works also suggested that a large basis set is crucial for the improvement, but even that does not always help. Because of the size of PQ, we were not able to check this in MP2 calculations.

While optimizing the geometry of PQ, we initially did not impose any symmetry on the molecule. This led to a practically planar geometry, with the dihedral angles not exceeding 0.03°. However, such a structure was considered nonsymmetrical by the Gaussian program, and all the modes were treated as belonging to the same symmetry species. For each model/basis set case, we repeated the calculations with planarity imposed by setting the values for all the dihedral angles equal to 0 or 180°. The differences between the two modes of calculations were quite significant. While the average and absolute average mean values did not change much (at most by 3 cm^{-1} for the case of B3LYP/6-31++G(3df,3pd) calculations), for some modes, the calculated frequencies were quite different. The most affected were the out-of-plane transitions, ν_{49} and ν_{37} in particular, for which differences exceeding 10 cm^{-1} were obtained. At the same time, the frequencies of in-plane modes were only weakly affected. Imposing the symmetry led to slight but systematic improvement of the agreement between theory and experiment, expressed by larger correlation coefficients and smaller SD values. The data presented in Tables 2−4 refer to symmetry-enforcing calculations. Naturally, imposing symmetry also resulted in much shorter computation times.

Using symmetry allowed us to compare the statistics separately for modes of a′ (in-plane, ip) and a″ (out-of-plane, oop) symmetry. A systematic difference was found in the accuracy of reproducing ip and oop vibrations: the frequencies of the former were predicted more precisely. The difference is difficult to observe for smaller basis sets but becomes visible for TZ and QZ sets. We will show below that this difference becomes much more dramatic when it comes to the predictions of the intensities.

4.2. Calculations of IR Intensities. In Figure 5, we show the experimental IR spectrum along with selected examples of IR intensity patterns predicted using various models/basis sets. Table 3 presents the statistics obtained for all types of calculations used in this work. Some general conclusions can be drawn on the basis of comparison between the computed and experimental spectra. First, the overall intensity pattern is reproduced correctly when using triple-ζ basis sets. For the case of double-ζ basis sets, the combination of B3LYP with Pople's basis sets does very well. Still, considerable differences are observed for different sizes of basis sets. The best agreement with experiment is obtained for 6-31+G(d), 6-31G(d,p), 6-31+G-(d,p), and 6-31++G(d,p). Adding polarization functions initially leads to a considerable decrease of both, correlation coefficients and standard deviations, as exemplified by the comparison of the results obtained with 6-31+G(d,p) and 6-31+G(2d,p). The

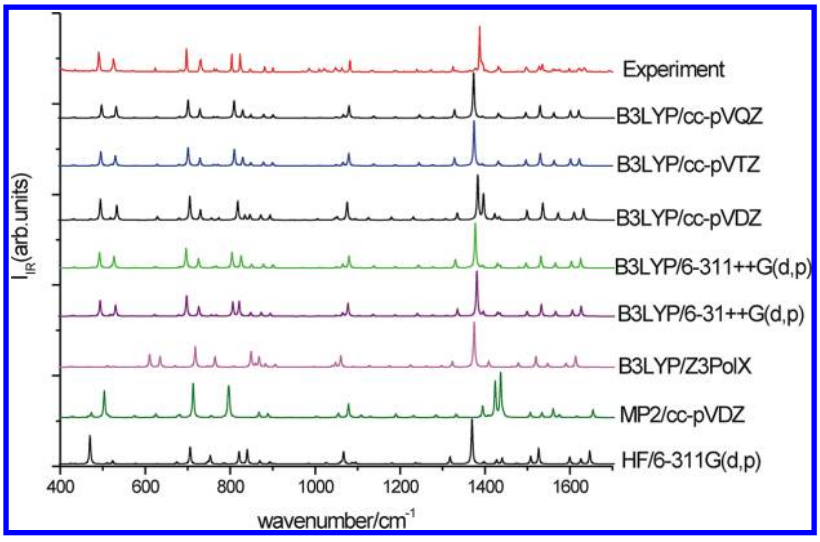

Figure 5. Comparison of IR intensity patterns calculated using different models with the experimental spectrum (top).

Table 3. Statistics for the Relative IR Intensities Calculated Using Different Models/Basis Sets

		all modes		ip modes		oop modes	
model	basis set	corr coeff	stand dev	corr coeff	stand dev	corr coeff	stand dev
HF	6-31G(d,p)	0.88575	0.094	0.96592	0.051	0.75799	0.140
	6-311G(d,p)	0.88950	0.089	0.95826	0.057	0.78257	0.120
MP2	cc-pVDZ	0.05735	0.264	0.01335	0.252	0.05912	0.296
B3LYP	6-31G	0.68990	0.148	0.97111	0.050	0.20448	0.246
	6-31G(d)	0.92997	0.067	0.98349	0.038	0.83368	0.088
	6-31+G(d)	0.92280	0.072	0.97351	0.044	0.82141	0.104
	6-31G(d,p)	0.93879	0.061	0.96910	0.048	0.93320	0.053
	6-31+G(d,p)	0.94765	0.059	0.97994	0.040	0.89068	0.077
	6-31++G(d,p)	0.96120	0.051	0.97999	0.040	0.94240	0.055
	6-31+G(2d,p)	0.87940	0.093	0.97792	0.042	0.69644	0.145
	6-31+G(2d,2p)	0.89536	0.085	0.97759	0.042	0.73688	0.132
	6-31+G(3d,3p)	0.92188	0.071	0.97943	0.042	0.80994	0.100
	6-31+G(3df,3pd)	0.90213	0.080	0.97937	0.041	0.74414	0.118
	6-31++G(3df,3pd)	0.91294	0.076	0.97944	0.041	0.77612	0.109
	cc-pVDZ	0.85559	0.107	0.87627	0.100	0.85715	0.097
	aug-cc-pVDZ	0.83998	0.116	0.95530	0.058	0.66215	0.190
	Z3PolX	0.74454	0.119	0.96067	0.055	0.82814	0.162
	Sadlej pVTZ	0.75853	0.183	0.71681	0.195	0.82814	0.162
	6-311G	0.72788	0.140	0.96278	0.054	0.31194	0.233
	6-311G(d)	0.88944	0.087	0.96593	0.050	0.75651	0.129
	6-311+G(d)	0.91387	0.079	0.97691	0.043	0.78790	0.124
	6-311G(d,p)	0.93738	0.063	0.97447	0.044	0.92296	0.062
	6-311+G(d,p)	0.93699	0.065	0.97878	0.042	0.85847	0.088
	6-311++G(d,p)	0.95569	0.054	0.97870	0.042	0.93056	0.058
	6-311+G(2d,p)	0.91740	0.076	0.97534	0.045	0.81106	0.108
	6-311+G(2d,2p)	0.92511	0.073	0.97564	0.045	0.83148	0.103
	6-311+G(3d,3p)	0.94559	0.061	0.97567	0.045	0.90575	0.069
	6-311+G(3df,3pd)	0.94909	0.057	0.97634	0.044	0.93291	0.053
	6-311++G(3df,3pd)	0.94928	0.057	0.97628	0.044	0.93583	0.052
	cc-pVTZ	0.93833	0.063	0.98030	0.042	0.88562	0.069
	aug-cc-pVTZ	0.91948	0.071	0.97140	0.046	0.82985	0.088
	cc-pVQZ	0.93558	0.064	0.97790	0.043	0.88904	0.071
CAM-B3LYP	6-31G(d,p)	0.85994	0.113	0.83568	0.127	0.94138	0.072
CAM-B3LYP	Z3PolX	0.74805	0.119	0.96267	0.055	0.26361	0.157
CAM-B3LYP	cc-pVTZ	0.92216	0.071	0.98039	0.041	0.82634	0.089
SVWN	6-311++G(d,p)	0.76089	0.094	0.93499	0.060	0.51629	0.234
	cc-pVTZ	0.77562	0.085	0.94601	0.053	0.50786	0.208
PBE	6-311++G(d,p)	0.82997	0.082	0.89516	0.082	0.71503	0.178
	cc-pVTZ	0.89585	0.053	0.97495	0.037	0.72944	0.115
PBE0	6-311++G(d,p)	0.79600	0.107	0.74747	0.153	0.87239	0.137
	cc-pVTZ	0.84928	0.077	0.85525	0.102	0.84425	0.120
M06	6-311++G(d,p)	0.95206	0.036	0.97543	0.038	0.95863	0.041
	cc-pVTZ	0.92525	0.044	0.97891	0.037	0.87745	0.063

correlation improves while adding more functions, but never reaches the accuracy obtained with more compact basis sets. A similar trend is observed for 6-311 basis sets, but now, practically the same agreement is observed for 6-311++G(d,p) and the much larger 6-311++G(3df,3dp). As was the case for frequency calculations, these results point to the importance of properly balancing the basis set.

The absolute necessity of including polarization functions for intensity calculations is illustrated by a huge difference between the results obtained with 6-31G and 6-31G(d) (Table 3). For calculations of frequencies (Table 2), the difference was not so dramatic.

The intensity predictions obtained with Dunning's cc-pVDZ and cc-PVTZ are definitely worse than those provided with Pople's basis sets. Adding diffuse functions (aug-cc-pVDZ and aug-cc-pVTZ) actually leads to a decrease in *R* and SD. The worst agreement between experiment and theory is obtained by MP2/cc-pVDZ; HF/6-311G(d,p) does much better (Figure 5).

Similarly as in the case of predicting vibrational frequencies, the CAM-B3LYP gives worse results than B3LYP. Interestingly, the difference in performance is remarkable when the 6-31G(d,p) basis set is used but rather minor for cc-pVTZ and Z3PolX.

The second general conclusion, which can be deduced from an inspection of Figure 5 and Table 3, regards a large difference in the accuracy of predicting the IR intensities for in-plane and out-of-plane modes. The former are reproduced extremely well even using modest basis sets, as illustrated by high and nearly constant values of the correlation coefficients (the exceptions in the case of cc-pVDZ and Sadlej's pVTZ are due to incorrect predictions of

dx.doi.org/10.1021/jp309618b | J. Phys. Chem. A 2012, 116, 11973−11986

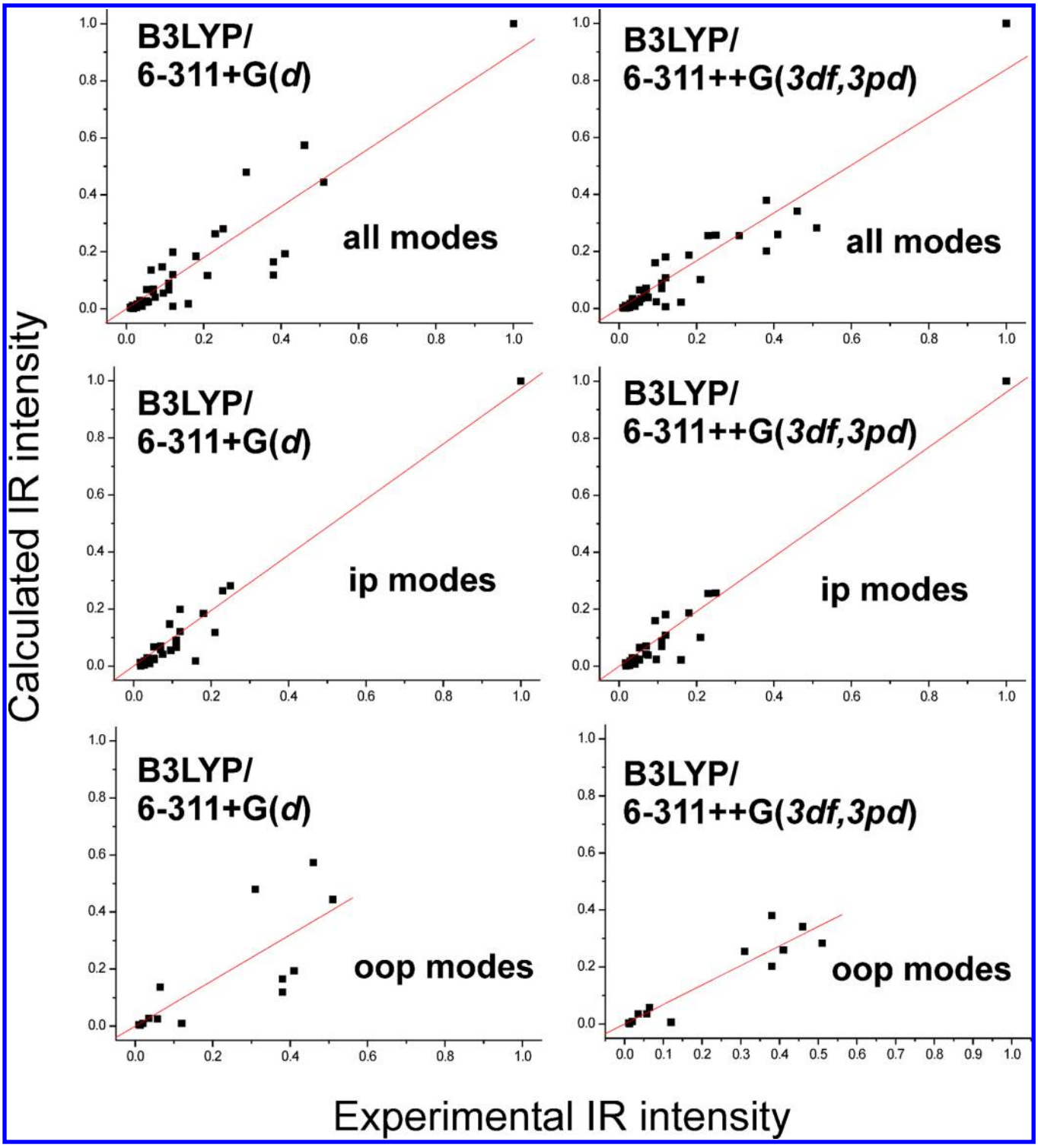

Figure 6. Correlations between predicted and measured relative IR intensities. Left, B3LYP/6-311+G(d), and right, B3LYP/6-311++G(3df,3pd) calculations. Top, all modes included, middle, only in-plane modes, and bottom, only out-of-plane vibrations.

two very intense transitions around 1400 cm^{-1}, whereas only one is experimentally observed). On the contrary, the intensities of oop vibrations are predicted poorly with double-ζ basis sets. Increasing the number of polarization functions does not help. It does, however, when triple-ζ basis sets are applied, as illustrated by a systematic increase of R and decrease of SD in the series 6-311G(d)−6-311++G(3df,3dp). Figure 6 shows a comparison between the results obtained using B3LYP/6-311+G(d) and B3LYP/6-311++G(3df,3dp). When only ip modes are considered, the correlation curves obtained using two different basis sets are very similar. In contrast, a separate analysis of the correlations for oop modes only reveals a significant improvement for the larger basis set.

4.3. Calculations of Raman Activities. The experimental Raman spectrum (Figures 1 and 7) has been measured with lower resolution than the IR absorption spectrum so that some

dx.doi.org/10.1021/jp309618b | J. Phys. Chem. A 2012, 116, 11973−11986

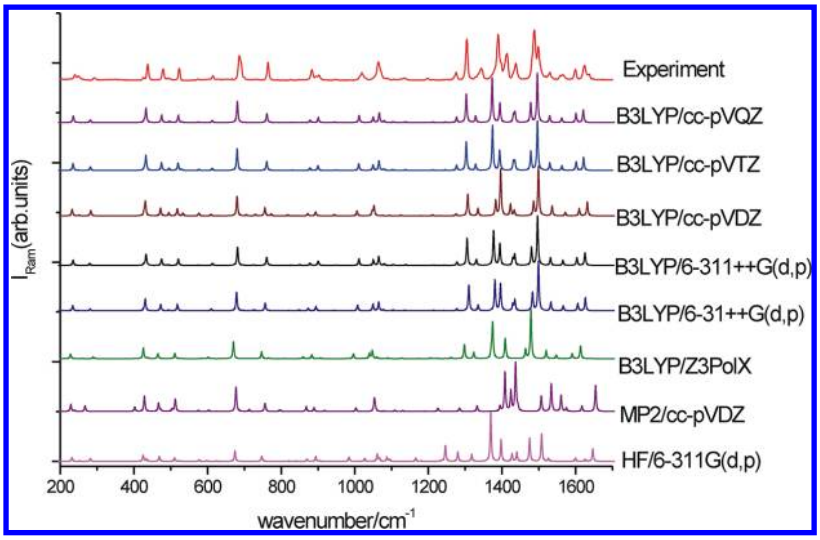

Figure 7. Comparison of Raman intensity patterns calculated using different models with the experimental spectrum (top).

peaks are difficult to separate. Therefore, while studying the correlations between experimental and predicted intensities, in four cases we used the experimental intensities obtained after integration over two Raman transitions. This was done for $\nu_{13} + \nu_{14}$, $\nu_{15} + \nu_{16}$, $\nu_{17} + \nu_{18}$, and $\nu_{28} + \nu_{29}$. These integrated intensities were correlated with the sums of calculated Raman intensities for the corresponding modes.

Figure 7 shows the experimental Raman spectrum compared with the theoretically predicted ones. The simulated and measured Raman spectra resemble each other even better than in the case of transitions observed in the IR. This is confirmed by comparing the values of *R* and SD in Tables 3 and 4. The origin of the better agreement in the case of Raman spectra becomes clear when one realizes that all the intense Raman transitions correspond to in-plane modes. It was not the case for IR, where the intense bands due to out-of-plane modes dominated the region below 1000 cm^{-1}. The weak intensities of the oop Raman-active modes lead to large errors in the experimental determination of their intensities. We did not succeed in getting reasonable correlations between the experimental and theoretically predicted Raman intensities of oop vibrations. This may be due to both experimental uncertainties and inaccurate computational predictions. Being unable to decide which source of error is larger, we did not include the separate correlations for oop modes in Table 4. We compared, however, the results obtained for all the modes with those obtained taking into account only the ip vibrations. The two sets of data are very similar, which is not surprising, given a very small contribution from the intensities of oop vibrations.

The simulated Raman intensities follow a somewhat different pattern than that observed for the IR. Extension of the basis set systematically improves the correlation, increasing *R* and decreasing SD. Also, the effect of adding diffuse functions is different: it now leads to an improvement, contrary to the case of IR intensities. Pople's and Dunning's basis sets reveal comparable accuracies in predicting the relative Raman intensities. As was the case for IR, CAM-B3LYP gives slightly worse results than B3LYP, the accuracy increasing in the same order: Z3PolX < 6-31G(d,p) < cc-pVTZ. A spectacular improvement is observed in the performance of Sadlej's basis sets, compared to the predictions of IR intensities.

Figure 8 shows the correlations between the experimental Raman intensities and the selected theoretical ones, calculated using double-, triple-, and quadruple-ζ basis sets. All four plots look very similar, reflecting comparable values of correlation coefficients and standard deviations (Table 4), suggesting that the convergence with regard to basis set has been achieved. As discussed above, this may be the case for the in-plane modes but not for the out-of-plane ones.

5. SUMMARY AND CONCLUSIONS

Reliable assignments of vibrational transitions in both IR and Raman spectra, obtained for the same sample of a molecule isolated in an inert, low temperature matrix have provided a unique data set for testing the performance of various theoretical models. Previous studies on this subject were usually limited to the data obtained for much smaller molecules under different experimental regimes. In a few cases of larger systems, e.g., thymine or anisole, the experimental spectrum was reconstructed from tabulated frequencies and activities;[1] for adenine, an experimental spectrum measured from a powder sample was used.[2]

The basic condition for a calculated IR or Raman spectrum to be considered helpful for the assignments is that the standard deviation in the predicted frequency is less than the average spacing between vibrational transitions. For this reason, SDs of the order of 20−30 cm^{-1} or even more are acceptable for small molecules but become prohibitive for systems with a larger number of vibrational modes. PQ exhibits 46 fundamental transitions in the region between 240 and 1620 cm^{-1}, not counting combinations and overtones. Some transitions are spaced less than 10 cm^{-1} apart. It is therefore of crucial importance to use methods for which the SDs are as small as possible. Fortunately, DFT calculations with B3LYP fulfill this criterion very well, for both Pople's and Dunning's DZ and TZ basis sets, but not for Sadlej's pVTZ and Z3PolX. Also, HF and MP2/cc-pVDZ calculations give errors that seem too large for reliable assignments. CAM-B3LYP, while less accurate than B3LYP, is acceptable, especially if used with cc-pVTZ. Among other functionals used, M06 is nearly as good as B3LYP; when used with 6-311++G(d,p) basis set, it even outperforms B3LYP in the simulations of IR intensities of out-of-plane transitions.

Table 4. Statistics for the Relative Raman Intensities Calculated Using Different Models/Basis Sets

		all modes		ip modes	
model	basis set	corr coeff	stand dev	corr coeff	stand dev
HF	6-31G(d,p)	0.88618	0.109	0.89080	0.129
	6-311G(d,p)	0.88713	0.110	0.89099	0.130
MP2	cc-pVDZ	0.82292	0.175	0.82422	0.211
B3LYP	6-31G	0.95188	0.090	0.95732	0.103
	6-31G(d)	0.95921	0.080	0.96340	0.092
	6-31+G(d)	0.97493	0.059	0.97786	0.068
	6-31G(d,p)	0.95974	0.080	0.96398	0.091
	6-31+G(d,p)	0.97504	0.059	0.97794	0.067
	6-31++G(d,p)	0.97535	0.059	0.97815	0.067
	6-31+G(2d,p)	0.97714	0.056	0.98022	0.064
	6-31+G(2d,2p)	0.97742	0.055	0.98052	0.062
	6-31+G(3d,3p)	0.97857	0.054	0.98148	0.061
	6-31+G(3df,3pd)	0.97694	0.056	0.97992	0.063
	6-31++G(3df,3pd)	0.97723	0.055	0.98022	0.063
	cc-pVDZ	0.96546	0.074	0.96924	0.084
	aug-cc-pVDZ	0.96997	0.062	0.97797	0.064
	Z3PolX	0.93267	0.091	0.94436	0.099
	Sadlej pVTZ	0.96702	0.067	0.97496	0.071
	6-311G	0.95579	0.085	0.96184	0.095
	6-311G(d)	0.96634	0.074	0.96951	0.085
	6-311+G(d)	0.97706	0.056	0.97991	0.064
	6-311G(d,p)	0.96631	0.074	0.96942	0.086
	6-311+G(d,p)	0.97620	0.058	0.97902	0.066
	6-311++G(d,p)	0.97627	0.058	0.97908	0.066
	6-311+G(2d,p)	0.97375	0.061	0.97739	0.068
	6-311+G(2d,2p)	0.97562	0.059	0.97929	0.066
	6-311+G(3d,3p)	0.97823	0.055	0.98125	0.062
	6-311+G(3df,3pd)	0.97696	0.057	0.98003	0.065
	6-311++G(3df,3pd)	0.97700	0.057	0.98006	0.065
	cc-pVTZ	0.97022	0.068	0.97308	0.079
	aug-cc-pVTZ	0.97874	0.054	0.98181	0.061
	cc-pVQZ	0.97308	0.064	0.97587	0.074
CAM-B3LYP	6-31G(d,p)	0.93854	0.093	0.94251	0.109
CAM-B3LYP	Z3PolX	0.90343	0.109	0.91126	0.126
CAM-B3LYP	cc-pVTZ	0.94584	0.086	0.94834	0.089
SVWN	6-311++G(d,p)	0.87404	0.122	0.87636	0.147
	cc-pVTZ	0.88603	0.121	0.88857	0.146
PBE	6-311++G(d,p)	0.96760	0.062	0.97053	0.071
	cc-pVTZ	0.97127	0.062	0.97440	0.071
PBE0	6-311++G(d,p)	0.96887	0.064	0.97142	0.075
	cc-pVTZ	0.96437	0.073	0.96702	0.086
M06	6-311++G(d,p)	0.96017	0.072	0.96260	0.084
	cc-pVTZ	0.96403	0.071	0.96656	0.082

It has long been recognized that reproducing experimental intensities in the vibrational spectra requires large, diffuse basis sets. The intensities depend on the derivatives of dipole moment and polarizability, which may be quite sensitive to the outer regions of electronic density. In principle, the results obtained for PQ confirm this view. However, a clear distinction has been found between the in-plane and out-of-plane modes. Quite reliable intensity patterns are obtained for the former already with rather limited basis sets. The accuracy of predicting intensities for out-of-plane modes strongly depends on the basis set, TZ clearly outperforming DZ. Because of very weak intensities of oop modes in Raman spectra, we could demonstrate this only for IR-active vibrations, but it seems that the requirements are even more stringent for the Raman spectra. The explanation of much poorer computational performance and of stronger basis set dependence in the case of out-of-plane transitions certainly requires further studies. To the best of our knowledge, this effect has not yet been discussed in the literature. In order to prove that it is not an artifact due to a particular combination of a pair of DFT functional/basis set, we have performed the calculations using six different functionals. Similar results have been obtained in all cases.

The clear difference in the accuracy of predicting intensities for transitions of different symmetry may provide another criterion for the assignments. A natural extension would be to exploit transition moment directions for the assignments, even in the case of vibrations of the same symmetry.

It would be tempting to compare our DFT results with those obtained using state-of-the-art methods, such as CCSD(T). Because of the prohibitive cost, we did not try CCSD(T)

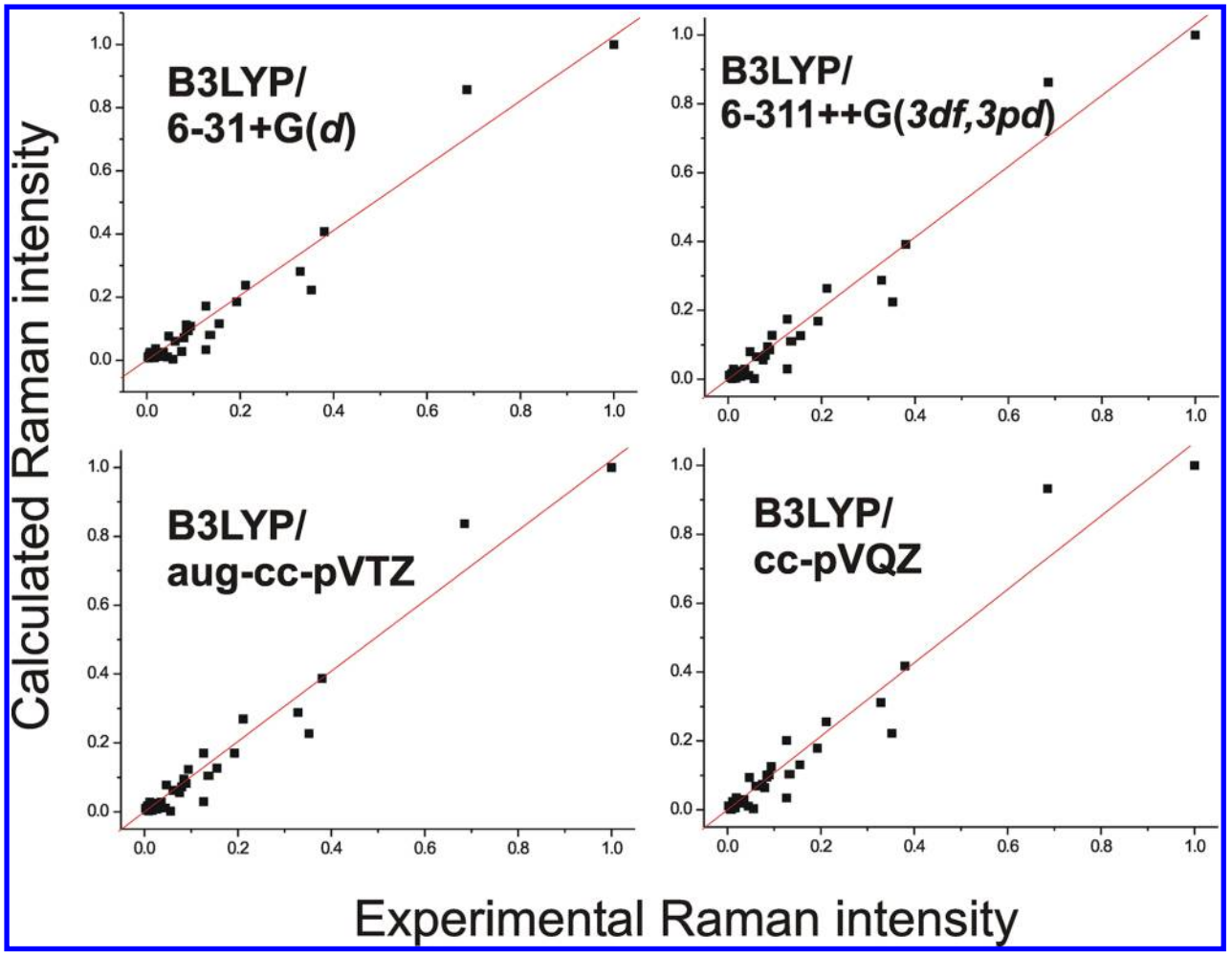

Figure 8. Correlations between predicted and measured relative Raman intensities. Top left, B3LYP/6-31+G(d), top right, B3LYP/6-311++G(3df,3pd), bottom left, B3LYP/aug-cc-pVTZ, and bottom right, B3LYP/cc-pVQZ calculations.

calculations, as it has been shown that, for quantitative predictions of IR intensities, basis sets of at least aug-cc-pVTZ quality are required.[3,37]

Our future plans include using PQ as a model in detailed studies of the vibrational structure in the lowest excited singlet state. Of particular interest will be the comparison of B3LYP and CAM-B3LYP functionals; the latter are recommended for studies of the electronic states with charge-transfer character, which is the case for PQ.[18]

Finally, we note that our investigations resulted in a large set of optimized geometries. Comparison with the experimental structure would contribute to characterizing the reliability of different theoretical methods for structural predictions. Unfortunately, PQ forms dimers in the crystalline phase[25] and therefore the comparison of the X-ray data with the results of calculations performed for the monomer would not be instructive. We intend to determine the exact geometry of monomeric PQ using microwave spectroscopy.

AUTHOR INFORMATION

Corresponding Author

*E-mail: waluk@ichf.edu.pl.

Notes

The authors declare no competing financial interest.

ACKNOWLEDGMENTS

The work was supported by the grant 3550/B/H03/2011/40 from the Polish National Science Centre. We acknowledge the computing grant G17-14 from the Interdisciplinary Centre for Mathematical and Computational Modeling of the Warsaw University and the NN 204 264 238 grant from the Ministry of Science and Higher Education. The Raman studies were supported by the European Union within European Regional Development Fund, through the Innovative Economy grant (POIG.01.01.02-00-008/08). R.P.T. thanks the National Science foundation (CHE-0714751) and the Robert A. Welch Foundation (E-621).

REFERENCES

(1) Zvereva, E. E.; Shagidullin, A. R.; Katsyuba, S. A. *J. Phys. Chem. A* **2011**, *115*, 63−69.
(2) Jiménes-Hoyos, C. A.; Janesco, B. G.; Scuseria, G. E. *Phys. Chem. Chem. Phys.* **2008**, *10*, 6621−6629.
(3) Galabov, B.; Yamaguchi, Y.; Remington, R. B.; Schaefer, H. F. I. *J. Phys. Chem. A* **2002**, *106*, 819−832.
(4) Halls, M. D.; Velkovski, J.; Schlegel, H. B. *Theor. Chem. Acc.* **2001**, *105*, 413−421.
(5) Halls, M. D.; Schlegel, H. B. *J. Chem. Phys.* **1999**, *111*, 8819−8824.
(6) Halls, M. D.; Schlegel, H. B. *J. Chem. Phys.* **1998**, 10587−10593.
(7) Thomas, J. R.; DeLeeuw, B. J.; Vacek, G.; Crawford, T. D.; Yamaguchi, Y.; Schaefer, H. F. I. *J. Chem. Phys.* **1993**, *99*, 403−416.

(8) Scott, A. P.; Radom, L. *J. Phys. Chem.* **1996**, *100*, 16502−16513.
(9) Wong, M. W. *Chem. Phys. Lett.* **1996**, *256*, 391−399.
(10) Kyrychenko, A.; Herbich, J.; Izydorzak, M.; Gil, M.; Dobkowski, J.; Wu, F. Y.; Thummel, R. P.; Waluk, J. *Isr. J. Chem.* **1999**, *39*, 309−318.
(11) Kyrychenko, A.; Herbich, J.; Izydorzak, M.; Wu, F.; Thummel, R. P.; Waluk, J. *J. Am. Chem. Soc.* **1999**, *121*, 11179−11188.
(12) Kyrychenko, A.; Herbich, J.; Wu, F.; Thummel, R. P.; Waluk, J. *J. Am. Chem. Soc.* **2000**, *122*, 2818−2827.
(13) Kyrychenko, A.; Stepanenko, Y.; Waluk, J. *J. Phys. Chem. A* **2000**, *104*, 9542−9555.
(14) Marks, D.; Zhang, H.; Borowicz, P.; Waluk, J.; Glasbeek, M. *J. Phys. Chem. A* **2000**, *104*, 7167−7175.
(15) Waluk, J. *Acc. Chem. Res.* **2003**, *36*, 832−838.
(16) Herbich, J.; Kijak, M.; Zielińska, A.; Thummel, R. P.; Waluk, J. *J. Phys. Chem. A* **2002**, *106*, 2158−2163.
(17) Kijak, M.; Zielińska, A.; Thummel, R. P.; Herbich, J.; Waluk, J. *Chem. Phys. Lett.* **2002**, *366*, 329−335.
(18) Kyrychenko, A.; Waluk, J. *J. Phys. Chem. A* **2006**, *110*, 11958−11967.
(19) Nosenko, Y.; Kunitski, M.; Thummel, R. P.; Kyrychenko, A.; Herbich, J.; Waluk, J.; Riehn, C.; Brutschy, B. *J. Am. Chem. Soc.* **2006**, *128*, 10000−10001.
(20) Nosenko, Y.; Kyrychenko, A.; Thummel, R. P.; Waluk, J.; Brutschy, B.; Herbich, J. *Phys. Chem. Chem. Phys.* **2007**, *9*, 3276−3285.
(21) Nosenko, Y.; Kunitski, M.; Riehn, C.; Thummel, R. P.; Kyrychenko, A.; Herbich, J.; Waluk, J.; Brutschy, B. *J. Phys. Chem. A* **2008**, *112*, 1150−1156.
(22) Del, V. J. C.; Dominguez, E.; Kasha, M. *J. Phys. Chem. A* **1999**, *103*, 2467−2475.
(23) Kyrychenko, A.; Waluk, J. *Biophys. Chem.* **2008**, *136*, 128−135.
(24) Krasnokutskii, S. N.; Kurkovskaya, L. N.; Shibanova, T. A.; Shabunova, V. P. *Zh. Strukt. Khim.* **1991**, *32*, 131−136.
(25) Gorski, A.; Gawinkowski, S.; Luboradzki, R.; Tkacz, M.; Thummel, R. P.; Waluk, J. *J. At. Mol. Opt. Phys.* **2012**, 236793.
(26) Taylor, C. A.; El-Bayoumi, M. A.; Kasha, M. *Proc. Natl. Acad. Sci. U.S.A.* **1969**, *63*, 253−260.
(27) Douhal, A.; Kim, S. K.; Zewail, A. H. *Nature* **1995**, *378*, 260−263.
(28) Folmer, D. E.; Wisniewski, E. S.; Castleman, A. W. *Chem. Phys. Lett.* **2000**, *318*, 637−643.
(29) Catalán, J.; Perez, P.; del Valle, J. C.; de Paz, J. L. G.; Kasha, M. *Proc. Natl. Acad. Sci. U.S.A.* **2002**, *99*, 5793−5798.
(30) Sekiya, H.; Sakota, K. *Bull. Chem. Soc. Jpn.* **2006**, *79*, 373−385.
(31) Takeuchi, S.; Tahara, T. *Proc. Natl. Acad. Sci. U.S.A.* **2007**, *104*, 5285−5290.
(32) Sekiya, H.; Sakota, K. *J. Photochem. Photobiol., C* **2008**, *9*, 81−91.
(33) Gil, M.; Waluk, J. *J. Am. Chem. Soc.* **2007**, *129*, 1335−1341.
(34) Kijak, M.; Nosenko, E.; Singh, A.; Thummel, R. P.; Waluk, J. *J. Am. Chem. Soc.* **2007**, *129*, 2738−2739.
(35) Becke, A. D. *J. Chem. Phys.* **1993**, *98*, 5648−5652.
(36) Lee, C.; Yang, W.; Parr, R. G. *Phys. Rev. B* **1988**, *37*, 785−789.
(37) Chapelli, C.; Biczysko, M. In *Computational Strategies for Spectroscopy. From Small Molecules to Nano Systems*; Barone, V., Ed.; John Wiley & Sons: Hoboken, NJ, 2012; pp 309−360.
(38) Yanai, T.; Tew, D. P.; Handy, N. C. *Chem. Phys. Lett.* **2004**, 51−57.
(39) Hohenberg, P.; Kohn, W. *Phys. Rev.* **1964**, *136*, B864−B871.
(40) Kohn, W.; Sham, L. J. *Phys. Rev.* **1965**, *140*, A1133−A1138.
(41) Slater, J. C. *The Self-Consistent Field for Molecular and Solids, Quantum Theory of Molecular and Solids*; McGraw-Hill: New York, 1974; Vol. *4*.
(42) Vosko, S. H.; Wilk, L.; Nusair, M. *Can. J. Phys.* **1980**, *58*, 1200−1211.
(43) Perdew, J. P.; Burke, K.; Ernzerhof, M. *Phys. Rev. Lett.* **1996**, *77*, 3865−3868.
(44) Adamo, C.; Barone, V. *J. Chem. Phys.* **1999**, *110*, 6158−6169.
(45) Zhao, Y.; Truhlar, D. G. *Theor. Chem. Acc.* **2008**, *120*, 215−241.
(46) Head-Gordon, M.; Pople, J. A.; Frisch, M. J. *Chem. Phys. Lett.* **1988**, *153*, 503−506.
(47) Hehre, W. J.; Ditchfield, R.; Pople, J. A. *J. Chem. Phys.* **1972**, *56*, 2257−2261.
(48) Hariharan, P. C.; Pople, J. A. *Chem. Phys. Lett.* **1972**, *16*, 217−219.
(49) Hariharan, P. C.; Pople, J. A. *Theor. Chim. Acta* **1973**, *28*, 213−222.
(50) Frisch, M. J.; Pople, J. A.; Binkley, J. S. *J. Chem. Phys.* **1984**, 3265−3269.
(51) Clark, T.; Chandrasekhar, J.; Spitznagel, G. W.; Schleyer, P. v. R. *J. Comput. Chem.* **1983**, *4*, 294−301.
(52) Krishnan, R.; Binkley, J. S.; Seeger, R.; Pople, J. A. *J. Chem. Phys.* **1980**, *72*, 650−654.
(53) Dunning, T. H. J. *J. Chem. Phys.* **1989**, *90*, 1007−1023.
(54) Sadlej, A. J. *Collect. Czech. Chem. Commun.* **1988**, *53*, 1995−2016.
(55) Benkova, Z.; Sadlej, A. J.; Oakes, R. E.; Bell, S. E. J. *J. Comput. Chem.* **2005**, *26*, 145−153.
(56) Frisch, M. J.; Trucks, G. W.; Schlegel, H. B.; Scuseria, G. E.; Robb, M. A.; Cheeseman, J. R.; Scalmani, G.; Barone, V.; Mennucci, B.; Petersson, G. A.; et al. *Gaussian 09*, revision B.01; Gaussian, Inc.: Wallingford CT, 2010.
(57) Minichino, C.; Barone, V. *J. Chem. Phys.* **1994**, *100*, 3717−3741.
(58) Tomasi, J.; Mennucci, B.; Cammi, R. *Chem. Rev.* **2005**, *105*, 2999−3093.
(59) Wu, F.; Chamchoumis, C. M.; Thummel, R. P. *Inorg. Chem.* **2000**, *39*, 584−590.
(60) Krauß, O.; Brutschy, B. *Chem. Phys. Lett.* **2001**, *350*, 427−433.
(61) Lommatzsch, U.; Gerlach, A.; Lahmann, C.; Brutschy, B. *J. Phys. Chem. A* **1998**, *102*, 6421−6435.
(62) Oakes, R. E.; Bell, P. M.; Benkova, Z.; Sadlej, A. J. *J. Comput. Chem.* **2004**, *26*, 154−159.
(63) Goodman, L.; Ozkabak, A. C.; Thakurt, S. N. *J. Phys. Chem.* **1991**, *95*, 9044−9058.
(64) Handy, N. C.; Maslen, P. E.; Amos, R. D.; Andrews, J. S.; Murray, C. W.; Laming, G. J. *Chem. Phys. Lett.* **1992**, *197*, 506−515.
(65) Handy, N. C.; Murray, C. W.; Amos, R. D. *J. Phys. Chem.* **1993**, *97*, 4392−4396.
(66) Maslen, P. E.; Handy, R. C.; Amos, R. D.; Jayatilaka, D. *J. Chem. Phys.* **1992**, *97*, 4233−4254.
(67) Michalska, D.; Zierkiewicz, W.; Bieńko, D. C.; Wojciechowski, W.; Zeegers-Huyskens, T. *J. Phys. Chem. A* **2001**, *105*, 8734−8739.